arXiv:1106.4429v1 [quant-ph] 22 Jun 2011

Quantum dynamics in light-harvesting complexes: Beyond the single-exciton limit

B. Cui, X. Y. Zhang and X. X. Yi
School of Physics and Optoelectronic Technology,
Dalian University of Technology, Dalian 116024 China
(Dated: June 23, 2011)

Primitive photosynthetic cells appear over three billion years prior to any other more complex life-forms, thus it is reasonable to assume that Nature has designed a photosynthetic mechanism using minimal resources but honed to perfection under the action of evolution. A number of different quantum models have been proposed to understand the high degree of efficient energy transport, most of them are limited to the scenario of single-exciton. Here we present a study on the dynamics in light-harvesting complexes beyond the single exciton limit, and show how this model describes the energy transfer in the Fenna-Matthew-Olson (FMO) complex. We find that the energy transfer efficiency above 90% under realistic conditions is achievable.

PACS numbers: 05.60.Gg, 03.65.Yz, 03.67.-a

I. INTRODUCTION

Light-harvesting complexes consist of several chromophores mutually coupled by dipolar interactions residing within a protein scaffold. Due to their mutual coupling, light-induced excitations on individual chromophores (sites) can undergo transfer from site to site. Excitation energy transfer (EET) has been an interesting subject for decades, not only for its phenomenal efficiency but also for its fundamental role in Nature [1]. Recent experiments on the exciton dynamics in photosynthetic bio-molecules (for example, the purple bacteria and the Fenna-Matthew-Olson complex) have brought a long-standing question again into the scientific focus that whether nontrivial quantum coherence effects exist in natural biological systems under physiological conditions [2, 3]. In fact, evidence of quantum coherence has been found, suggesting that nontrivial quantum effects may be at the heart of its remarkable excitation transport efficiency [4].

Inspired by these experimental results, several studies have attempted to unravel the precise role of quantum coherence in the EET of light-harvesting complexes [5–13], and environmental decoherence and noise have been found to play a crucial role [5–8, 14, 15]. In these studies, the system is assumed to be initialized with a single excitation in site 1. This may not be realized precisely under experimental or natural operating conditions. Considering that primitive photosynthetic cells appeared over three billion years prior to any other more complex life-forms, it is not illogical to assume that nature has designed a photosynthetic mechanism using minimal resources to gain maximal energy under the action of evolution. In this perspective, a model which allows a freedom to control the number of excitations in the complex at any time should be taken into account.

This paper extends the theoretical formulation presented in a recent paper [7] to a scenario of multi-exciton and further examines issues relevant for realistic light-harvesting complexes. To this end, we identify the FMO complex with coupled cavities and introduce two fundamental decoherence mechanisms (i.e., dephasing and dissipation) into the system. Under the semi-classical approach and with the quantum theory, we calculate respectively the excitation transfer efficiency. The decoherence rates that are optimal to the ETE are found by numerical simulation of the equation of motion. With the optimal decoherence rates, the time evolution of population on each site is presented. We found that the optimal decoherence rates weakly depend on the initial excitation number on site 1. The non-local decoherence slightly alter the ETE, indicating that local decoherence dominates the energy transfer in the FMO complex.

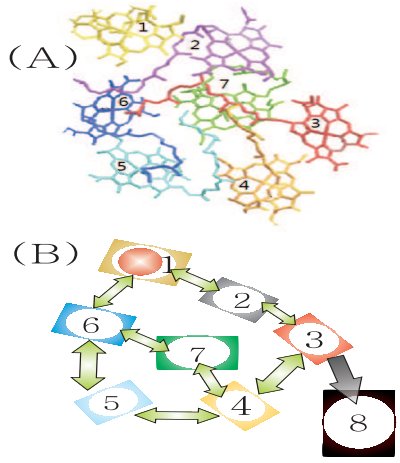

FIG. 1: (A) The disordered structure of the Fenna-Matthews-Olson (FMO) complex. The FMO complex acts as an energy transfer channel in green sulphur bacteria guiding excitations from the lightharvesting antenna at site 1 to the reaction center at site 8. This picture is re-produced from [15]. (B) The model to describe the FMO complex. Arrows between the cavities represent cavity-cavity couplings. Only couplings above 15 cm^{-1} are shown. The reaction center is modeled by the cavity, numbered 8, that is irreversibly coupled to the site 3. It is worth bearing in mind that the coupling between cavity 1 and cavity 6 is week with respect to the other couplings shown in the figure.

The paper is organized as follows. In Sec. II we introduce the theoretical model for the FMO dynamics and define the excitation transfer efficiency (ETE) used here. Then, we analyze the ETE and the dynamics in the FMO complex with both semi-classical and quantum theories in Sec.III. Finally, we conclude our results in Sec. IV.

II. MODEL DESCRIPTION

In photosynthetic antennae, sunlight is absorbed by pigments and the excitation energy is transferred to the photosynthetic reaction center. The locations for these processes are physically and physiologically separated, suggesting that two-level systems are good to model the pigments with single-exciton but not enough for pigments with many excitations. To describe the light-harvesting process with many excitations on each site, we model the FMO complex by a coupled 8-cavity system, see Fig. 1. The effective dynamics can be described by a Hamiltonian describing the coherent exchange of excitations between chromophores or sites,

$$H=\sum_{j=1}^{7}\omega_j a_j^\dagger a_j+\sum_{i,j=1}^{7}g_{ij}(a_i^\dagger a_j+a_i a_j^\dagger),\ i\neq j\ , \qquad (1)$$

where $a_j^\dagger$ (a_j) are the creation (annihilation) operators for site j, ω_j is the local site excitation energy, and g_{ij} denotes the hopping rate of an excitation between the sites i and j. In the site basis, we follow [16] and employ the Hamiltonian matrix elements (in units of cm^{-1})

$$H=\begin{pmatrix} \mathbf{215} & \mathbf{-104.1} & 5.1 & -4.3 & 4.7 & \mathbf{-15.1} & -7.8 \\ \mathbf{-104.1} & \mathbf{220.0} & \mathbf{32.6} & 7.1 & 5.4 & 8.3 & 0.8 \\ 5.1 & \mathbf{32.6} & 0.0 & \mathbf{-46.8} & 1.0 & -8.1 & 5.1 \\ -4.3 & 7.1 & \mathbf{-46.8} & \mathbf{125.0} & \mathbf{-70.7} & -14.7 & \mathbf{-61.5} \\ 4.7 & 5.4 & 1.0 & \mathbf{-70.7} & \mathbf{450.0} & \mathbf{89.7} & -2.5 \\ \mathbf{-15.1} & 8.3 & -8.1 & -14.7 & \mathbf{89.7} & \mathbf{330.0} & \mathbf{32.7} \\ -7.8 & 0.8 & 5.1 & \mathbf{-61.5} & -2.5 & \mathbf{32.7} & \mathbf{280.0} \end{pmatrix}. \qquad (2)$$

Here the zero energy has been shifted by 12230 cm^{-1} for all sites, corresponding to a wavelength of $\sim$ 800nm. We note that in units of $\hbar=1$, 1 ps^{-1}=5.3 cm^{-1}. Then by dividing g_{ij} and ω_j by 5.3, all elements of the Hamiltonian are rescaled in units of ps^{-1}. We can find from the Hamiltonian H that in the Fenna-Matthew-Olson complex (FMO), there are two dominating EET pathways: $1\to 2\to 3$ and $6\to(5,7)\to 4\to 3$ (see figure 1). Although the nearest neighbor terms dominate the site to site coupling, significant hopping matrix elements exist between more distant sites. This indicates that coherent transport itself may not explain why the excitation energy transfer is so efficient.

To obtain high energy transfer efficiency in the EET process, forward and backward energy transfer rates as well as the dissipation induced by the *hot and wet* surrounding environment need to satisfy a detailed balance condition. In the weak dissipation regime, the Lindblad master equation that is able to reliably describe exciton dissipative dynamics reads,

$$\begin{aligned}\frac{d\rho}{dt} &= -i[H,\rho]+\mathcal{L}_{deph}(\rho)+\mathcal{L}_{diss}(\rho)\\ &\quad +\mathcal{L}_{NLdeph}(\rho)+\mathcal{L}_{NLdiss}(\rho)+\mathcal{L}_8(\rho)\ , \qquad (3)\end{aligned}$$

where $\mathcal{L}_{diss}(\rho)$ describes dissipation terms, and $\mathcal{L}_{deph}(\rho)$ denotes dephasing terms. $\mathcal{L}_{NLdeph}(\rho)$ and $\mathcal{L}_{NLdiss}(\rho)$ represent non-local dephasing and dissipation, respectively. Here,

$$\mathcal{L}_{diss}(\rho)=\sum_{j=1}^{7}\Gamma_j(2a_j\rho a_j^\dagger-\rho a_j^\dagger a_j-a_j^\dagger a_j\rho)\ , \qquad (4)$$

$$\mathcal{L}_{deph}(\rho)=\sum_{j=1}^{7}\gamma_j(2n_j\rho n_j-\rho n_j n_j-n_j n_j\rho), \qquad (5)$$

$$\mathcal{L}_{NLdiss}(\rho)=\sum_{i,j=1}^{7}\Gamma_{ij}(2a_i\rho a_j^\dagger-\rho a_j^\dagger a_i-a_j^\dagger a_i\rho), i\neq j, \qquad (6)$$

and

$$\mathcal{L}_{NLdeph}(\rho)=\sum_{i,j=1}^{7}\gamma_{ij}(2n_i\rho n_j-\rho n_j n_i-n_j n_i\rho), i\neq j, \qquad (7)$$

where $n_j=a_j^\dagger a_j$ denotes the exciton number operator for site j.

The local decoherence may come from the couplings of the sites to individual environments, whereas the non-local decoherence $\mathcal{L}_{NLdeph}(\rho)$ and $\mathcal{L}_{NLdiss}(\rho)$ can be understood as a result of the interaction between the site and a common environment. From a quantum physical perspective, environmental radiations whose wavelength is larger than the length-scale of the FMO molecule ($\sim$ 8

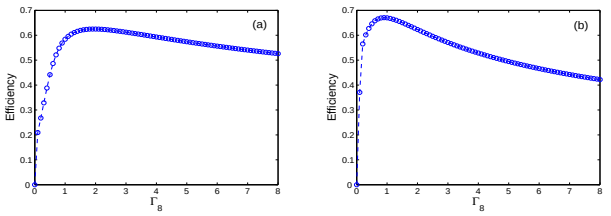

FIG. 2: Energy transfer efficiency versus Γ_8 without decoherence ($\Gamma_j = \gamma_j = \Gamma_{ij} = \gamma_{ij} = 0$, i, j=1,2,...,7). (a) For semi-classical approach and, (b) for quantum theory. $N_0 = 100$ is taken for this plot.

nm) are reasonably assumed to take the role of a common environment. Thus the decoherence considered here is reasonable.

Recent work [3] suggests that it is the site 3 that couples to the reaction center. The total transfer of excitations into the reaction center is measured by the population in the center, numbered 8, which is populated by an irreversible decay process with rate Γ_8 from the site 3. We phenomenologically model this irreversible process by the Lindblad operator,

$$\mathcal{L}_8(\rho) = \Gamma_8(2a_8^\dagger a_3 \rho a_3^\dagger a_8 - \rho a_3^\dagger a_3 a_8 a_8^\dagger - a_3^\dagger a_3 a_8 a_8^\dagger \rho) \ . \quad (8)$$

To match the observation in experiments, we assume there are N_0 excitations initially in site 1. The model is completed by introducing a quantity by which we measure the energy transfer efficiency. The rescaled population in the reaction center given by

$$p_8 = \frac{n_8(T)}{N_0} = \frac{\mathrm{Tr}(a_8^\dagger a_8 \rho(T))}{N_0}, \quad (9)$$

at a specific time T is good for this purpose.

Note that the reaction center is directly connected only to site 3. The decoherence rate Γ_8 plays an essential role in the excitation transfer. In the next section, we will use the decoherence rates to optimize the transfer efficiency defined in Eq.(9). Several cases are considered, in each case Γ_8 can not be zero, because null Γ_8 leads to zero transfer efficiency.

III. ENERGY TRANSFER EFFICIENCY

Having this model, we now explore the energy transport in the FMO complex. Two approaches are considered. In the semi-classical approach, we will use the approximation $\langle a_j^\dagger a_j \rangle = |\alpha_j|^2$ with $\alpha_j = \mathrm{Tr}(\rho a_j)$. Whereas in the quantum regime, we approximate $\langle a_8^\dagger a_8 a_3^\dagger a_3 \rangle$ as $\langle a_8^\dagger a_8 \rangle \langle a_3^\dagger a_3 \rangle$. By these approximations, we can derive the equation of motion for the system and calculate the energy transfer efficiency. We first focus on the case where only local decoherence exists, namely $\Gamma_{ij} = 0$ and $\gamma_{ij} = 0$, then move to the case with non-local decoherence. The energy transfer time is taken to $T = 5$ ps^{-1},

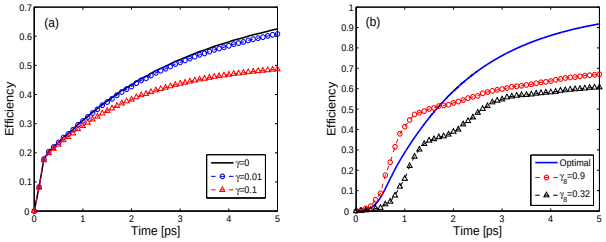

FIG. 3: (color online) Efficiency as a function of time, only local decoherence is considered. Figure (a) is the results with semi-classical approach, where black solid line is for the null decoherence case ($\Gamma_j = \gamma_j = 0$), and blue circle and red triangle are for $\Gamma_j = 0$, $\gamma_j = 0.01$ and $\Gamma_j = 0$, $\gamma_j = 0.1$, respectively, $j = 1, 2, ..., 7$. Other parameters chosen are $\Gamma_8 = 1.94$ and $N_0 = 100$. (b) is the efficiency from quantum theory. Blue solid line stands for optimal efficiency with rates $(\gamma_1, \gamma_2, \gamma_3, \gamma_4, \gamma_5, \gamma_6, \gamma_7)$ =(0.74, 24, 0, 5.2, 50.6, 0, 15), $\Gamma_8 = 0.32$ and the other $\Gamma_j = 0.0005$. The efficiency reaches its maximum 91.77% that is optimized at 5 ps. Red circle and black triangle lines represent the null decoherence case with $\Gamma_8 = 0.9$ (the corresponding efficiency is 67.06%) and $\Gamma_8 = 0.32$ (corresponding to efficiency 60.73%), respectively.

which is the relevant time scale in recent experiment [3]. Our results suggest that it is the careful interplay of quantum mechanical features and the unavoidable couplings to environment that will leads to the optimal system performance. In particular, the local decoherence dominates and actually helps the excitation transfer, as we will show below.

A. Semi-classical approach

Define $\alpha_j = \mathrm{Tr}(\rho a_j)$ and $n_8 = \mathrm{Tr}(a_8^\dagger a_8 \rho)$, the master equation Eq. (3) yields,

$$\begin{aligned}
\dot{\alpha}_j &= -i(\omega_j \alpha_j + 2\sum_{k\neq j} g_{jk}\alpha_k) - \Gamma_j \alpha_j - \gamma_j \alpha_j - \sum_{k\neq j} \Gamma_{jk}\alpha_k, j \neq 3, 8, \\
\dot{\alpha}_3 &= -i(\omega_3 \alpha_3 + 2\sum_{k\neq 3} g_{3k}\alpha_k) - \Gamma_3 \alpha_3 - \gamma_3 \alpha_3 - \sum_{k\neq 3} \Gamma_{3k}\alpha_k - \Gamma_8(n_8+1)\alpha_3,
\end{aligned}$$

$$\dot{n}_8 = 2\Gamma_8|\alpha_3|^2(n_8+1), \tag{10}$$

where the dot represents time derivative, and the time arguments have been omitted to shorten the representation. To obtain Eq. (10), the approximation $\langle a_j^\dagger a_j\rangle = |\alpha_j|^2$ in the last equation of Eq. (10) has been made. These equations compose a closed set of equations governing the dynamics of the FMO complexes.

As shown in [7], a completely coherent dynamics is often not most ideal for the excitation transfer from the chromophores to the reaction center, and hence the coherence solely can not explain the very high exciton transfer efficiency observed in experiments. Our model confirms this result. In fact, with $\Gamma_j = \gamma_j = \Gamma_{ij} = \gamma_{ij} = 0$ $(i, j = 1, 2, ..., 7)$, the transfer efficiency arrives at its maximum 0.625 with $\Gamma_8 = 1.94$ ps^{-1} (see Figs. 2(a) and 3(a)).

Further numerical simulations show that under the semi-classical approximation, dissipation and dephasing play similar roles in the dynamics of FMO, see Eq. (10). Numerical simulations show that neither dissipation nor dephasing can improve the energy transfer efficiency under the semi-classical approximation (see Fig. 3(a)). This is due to the fact that dephasing and dissipation play a same role in the dynamics under the semi-classical approach, see Eq. (10). Remind that the local dissipation always spoil the exciton transfer from sites to the reaction center, it is not difficult to understand why the decoherence can not help the exciton transfer within the semi-classical approach.

B. Quantum theory

We now examine whether the quantum theory can explain the high exciton transfer efficiency. For this purpose, we approximate $\langle a_8^\dagger a_8 a_3^\dagger a_3\rangle$ as $\langle a_8^\dagger a_8\rangle\langle a_3^\dagger a_3\rangle$. Define $n_{mm} = \mathrm{Tr}(\rho a_m^\dagger a_m)$, and $n_{mn} = \mathrm{Tr}(\rho a_m^\dagger a_n)$. We obtain from Eq. (3)

$$\begin{aligned}
\dot{n}_{mm} &= -i\sum_j g_{mj}n_{mj} + i\sum_j g_{mj}n_{jm} - 2\Gamma_m n_{mm} - \sum_j \Gamma_{mj}(n_{jm}+n_{mj}),\\
\dot{n}_{mn} &= i(\omega_m-\omega_n)n_{mn} + i\sum_j g_{jm}n_{jn} - i\sum_j g_{jn}n_{mj} - (\Gamma_m+\Gamma_n+\gamma_m+\gamma_n-2\gamma_{mn})n_{mn}\\
&\quad -\sum_j \Gamma_{mj}n_{jn} - \sum_j \Gamma_{nj}n_{mj} - a\Gamma_8 n_{mn}(n_{88}+1), m\neq n,\\
\dot{n}_{88} &= 2\Gamma_8 n_{33}(n_{88}+1),
\end{aligned} \tag{11}$$

where $a = 1$ for $m = 3$ or $n = 3$, and $a = 2$ for $m = n = 3$, otherwise $a = 0$. Eq. (11) is accurate when $\langle a_8^\dagger a_8 a_3^\dagger a_3\rangle = \langle a_8^\dagger a_8\rangle\langle a_3^\dagger a_3\rangle$. In fact, our numerical simulations show that this is exactly the case for small number of exciton. For instance, with $N_0 = 1$ or 2, Monte Carlo simulations show that $\langle a_8^\dagger a_8 a_3^\dagger a_3\rangle - \langle a_8^\dagger a_8\rangle\langle a_3^\dagger a_3\rangle = 0$. On the other hand, our model backs to the two-level model for the FMO complex when $N_0 = 1$[7], and the numerical results given by Eq. (11) is in agreement with that in [7]. It is difficult to prove $\langle a_8^\dagger a_8 a_3^\dagger a_3\rangle - \langle a_8^\dagger a_8\rangle\langle a_3^\dagger a_3\rangle = 0$ for any N_0. Fortunately, the site 3 and the reaction center 8 are connected only through the irreversible process $\mathcal{L}_8(\rho)$, and this term unlikely creates entanglement between site 3 and 8. Therefore if site 3 and 8 are initially in a separable state, then they will remain unentangled forever. For site 3 and 8 in separable states, $\langle a_8^\dagger a_8 a_3^\dagger a_3\rangle = \langle a_8^\dagger a_8\rangle\langle a_3^\dagger a_3\rangle$ holds true. This is not a proof, so we prefer to treat $\langle a_8^\dagger a_8 a_3^\dagger a_3\rangle = \langle a_8^\dagger a_8\rangle\langle a_3^\dagger a_3\rangle$ as an approximation.

We first study the case where only local decoherence exists, namely, $\Gamma_{ij} = \gamma_{ij} = 0$. By numerically solving Eq. (11), we find that without decoherence the maximal energy transfer efficiency is 67.06% (see Fig. 2(b)), which is a bit larger than that given by the semi-classical approach. However, with the assistance of local decoherence, an efficiency over ninety percent can be obtained (See Fig. 3(b)). In order to obtain such a high energy transfer efficiency, we have to optimize the 15 decoherence rates (Γ_j, γ_j, and Γ_8, $j = 1, 2, 3, ..., 7$), this is a time-consuming task. To save the computer time, we specify the dissipation rates to $\Gamma_j = 0.0005$ for each site to match the measured life time in experiments, which is the order of nanosecond [3] for the light-harvesting system. The optimal dephasing rates for highest efficiency are found numerically as $(\gamma_1, \gamma_2, \gamma_3, \gamma_4, \gamma_5, \gamma_6, \gamma_7)$ =(0.74, 24, 0, 5.2, 50.6, 0, 15) and $\Gamma_8 = 0.32$, the corresponding efficiency is 91.77% for initial $N_0 = 100$ on set 1.(see Fig. 3). Further numerical simulations show that the energy transfer efficiency can reach over ninety percent for al-

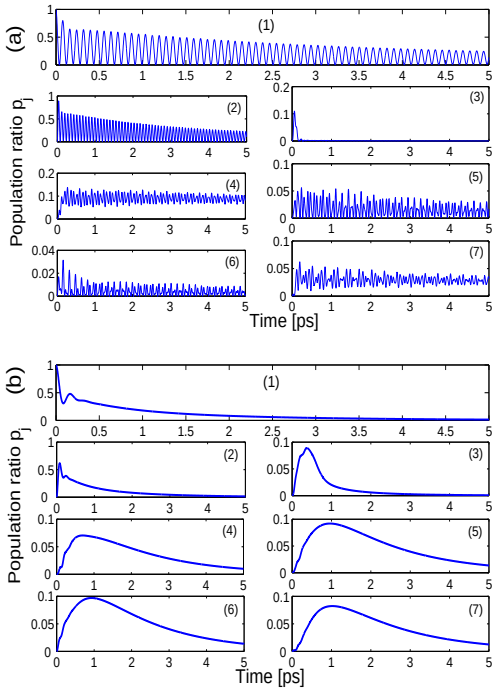

FIG. 4: Population ratio of j-th site defined by $p_j = \frac{n_{jj}}{N_0}$ as a function of time (number 1,2,...,7 label the sites). (a) is for the semi-classical approach. And (b) is for the quantum theory. Dissipation and dephasing rates are the same as those which optimize the efficiency with initial exciton number $N_0 = 100$.

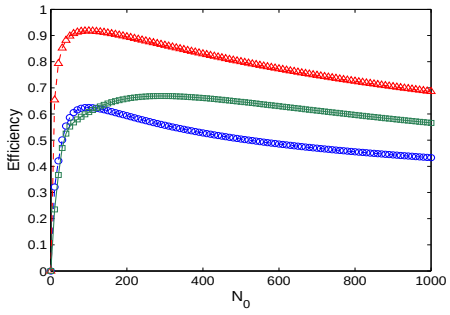

FIG. 5: (color online) Efficiency versus excitation number N_0 Parameters are chosen in such a way that the efficiency is optimized with $N_0 = 100$. $(\gamma_1, \gamma_2, \gamma_3, \gamma_4, \gamma_5, \gamma_6, \gamma_7)$ =(0.74, 24, 0, 5.2, 50.6, 0, 15), $\Gamma_8 = 0.32$ and $\Gamma = 0.0005$ is for the red triangle line. In contrast, we plot the results without decoherence in green square and blue circle lines with $\Gamma_8 = 0.32$ (quantum) and $\Gamma_8 = 1.94$ (semi-classical), respectively. The later two Γ_8 optimize the transfer efficiency for null decoherence case.

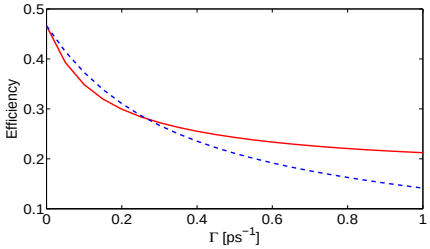

FIG. 6: (color online) Efficiency as a function of local dissipation rate ($\Gamma_j = \Gamma, j = 1, 2, ..., 7$). This figure is plotted to show the effect of non-local decoherence on the transfer efficiency. Red solid line represents a case with nonlocal dissipation ($\Gamma_{ij} = \Gamma$), whereas the blue dash line is for the case without nonlocal dissipation ($\Gamma_{ij} = 0$), $i, j = 1, 2, ..., 7$. Other parameters chosen are $\Gamma_8 = 6$, $\gamma_j = 0$, and $\gamma_{ij} = 0$.

most arbitrary exciton number N_0 (from 1 to 10000) on site 1, though the optimal dephasing rates are different. With the optimal dephasing rates, the ratio of exciton number on each site to the total number of exciton (defined as $p_m = \frac{n_{mm}}{N_0}$) is plotted, see Fig.4 (b). We find that after a rapid increasing (except for site 1), the exciton number decreases for each site, indicating that most of the exciton are transferred to the reaction center at site 8 (see Fig. 4(b)). In contrast, the dynamics from the semi-classical approach (see Fig. 4(a)) is also plotted. More oscillations can be observed, leading to less population transfer to the reaction center.

It is interesting to note that the optimal decoherence rates obtained for different exciton number N_0 are approximately the same values. To show this point we have plotted in Fig. 5 the efficiency as a function of the exciton number N_0, the decoherence rates used in this figure are optimal for $N_0 = 100$. Clearly, the decoherence rates optimal for $N_0 = 100$ can also result in high transfer efficiency for a wide range of N_0. For instance, the efficiency remains above ninety percent at $N_0 = 200$ with the optimal decoherence rates for $N_0 = 100$. This observation suggests that the high efficient energy transport, which has been found for a fixed excitation number remains valid for other experimental and natural operating conditions. Biologically, this means the light-harvesting system is robust against the number of photon captured at site 1. Meanwhile, we observe that the dependence on small N_0 (see Fig. 5) is stronger than the dependence on large N_0, suggesting that the transfer efficiency is sensitive to the variations of small N_0. This feature can be understood by carefully examining Eq. (11). Clearly, the losing rate of population on site 3 depends on the population in the reaction center, n_{88}. As a back action, the gaining rate of population on the reaction center depends on n_{33}.

C. Effect of non-local decoherence

In this section, we examine the effect of non-local decoherence on the energy transfer efficiency and the dynamics of the FMO complex. When taking Eqs. (6) and (7) into account, we must guarantee that the non-local decoherence terms with rates Γ_{ij} and γ_{ij} should keep the positivity and trace preserving of the density matrix [7]. For

this reason, we choose all Γ_{ij} and γ_{ij} positive to optimize the transfer efficiency. We find that the energy transfer efficiency can be increased by properly choosing non-local dephasing rates. For example, with the optimized local decoherence rates ($\{\gamma_1, \gamma_2, \gamma_3, \gamma_4, \gamma_5, \gamma_6, \gamma_7\}$ =$\{0.74,\ 24,\ 0,\ 5.2,\ 50.6,\ 0,\ 15\}$, $\Gamma_8 = 0.32$, and $\Gamma = 0.0005$), the efficiency can be increased from 91.77% without non-local decoherence to 91.907% with non-local decoherence rates, $(\gamma_{17}, \gamma_{71}, \gamma_{25}, \gamma_{52})$=(0.74,0.74,24,24) and $\gamma_{ij} = 0, \{i, j\} \neq \{1, 2, 5, 7\}$. Extensive numerical simulations show that energy transfer efficiency can not be increased by weak non-local decoherence Γ_{ij} (orders of ns^{-1}), but strong non-local decoherence can improve the energy transfer efficiency as Fig. 6 shows.

IV. CONCLUSION

In summary, we have studied the dynamics in light-harvesting complexes beyond the single exciton limit and optimized the energy transfer efficiency in the Fenna-Matthew-Olson (FMO) complex. To describe the multi-excitation scenario, we have proposed a new model for the propagation of excitation transfer, the model consists of 7 coupled cavities and a reaction center. Four types of decoherence, including local dephasing, local dissipation, nonlocal dephasing and nonlocal dissipation are considered. To match the life-time of exciton observed in experiment, we fixed the local dissipation rates to 0.0005 ps^{-1}. The local dephasing rates that optimizes the transfer efficiency are given by numerical simulation. We find that for multi-excitation case, the energy transfer efficiency can be over 90% under realistic conditions. Non-local decoherence can slightly increase the efficiency, but it seems not important in the light-harvesting mechanism. Moreover, we find that the transfer efficiency is not sensitive to the initial excitation number at site 1. This suggests that the light-harvesting antenna may capture more photons once and the experimental conditions are flexible to simulate the light-harvesting in FMO complex.

We are indebted to C. P. Sun for suggestions and stimulating talks. Discussions with J. Cheng and S. Yi are acknowledged. This work is supported by NSF of China under grant Nos 61078011 and 10935010, as well as the National Research Foundation and Ministry of Education, Singapore under academic research grant No. WBS: R-710-000-008-271.

[1] T. Förster, Ann. Phys. (Leipzig), 2, 55 (1948); A. G. Redfield, Adv. Magn. Reson. 1, 1 (1965); M. Grover and R. Silbey, J. Chem. Phys. 54, 4843 (1971); G. D. Scholes, Annu. Rev. Phys. Chem 54, 57 (2003).
[2] H. Lee, Y-C. Cheng, and G. R. Fleming, Science 316, 1462 (2007); V. I. Prokhorenko et al., J. Phys. Chem. B 106, 9923 (2002).
[3] J. Adolphs and T. Renger, Biophys. J. 91, 2778, (2006).
[4] G. S. Engel, T.R. Calhoun, E.L. Read, T.-K. Ahn, T. Manal, Y.-C. Cheng, R.E. Blankenship, and G.R. Fleming, Nature 446, 782 (2007).
[5] M. Mohseni, P. Rebentrost, S. Lloyd, and A. Aspuru-Guzik, J. Chem. Phys. 129, 174106 (2008).
[6] M.B. Plenio and S.F. Huelga, New J. Phys. 10, 113019 (2008).
[7] F. Caruso, A.W. Chin, A. Datta, S.F. Huelga, and M.B. Plenio, J. Chem. Phys. 131, 105106 (2009).
[8] A.W. Chin, A. Datta, F. Caruso, S.F. Huelga, and M.B. Plenio, New J. Phys. 12, 065002 (2010).
[9] A. Olaya-Castro, C.F. Lee, F.F. Olsen, and N.F. Johnson, Phys. Rev. B 78, 085115 (2008).
[10] A. Ishizaki and G.R. Fleming, Proc. Natl. Acad. Sci. 106, 17255 (2009).
[11] S. Yang, D. Z. Xu, Z. Song, C. P. Sun, J. Chem. Phys. 132, 234501 (2010).
[12] S. Hoyer, M. Sarovar, and K.B. Whaley, e-print arXiv:0910.1847 (2009).
[13] M. Sarovar, Y. C. Cheng, and K. B. Whaley, Phys. Rev. E **83**, 011906 (2011).
[14] F. Caruso, S.F. Huelga, and M.B. Plenio, e-print arXiv:1003.5877 (2010).
[15] A. Shabani, M. Mohseni, H. Rabitz, and S. Lloyd, e-print arXiv: 1103.3823.
[16] See the third column in table 2, and the second column in table 4 of Ref. [3].